Analysis of the Photoneutron Field Near the THz Dump of the CLEAR Accelerator at CERN With SEU Measurements and Simulations

Giuseppe Lerner, Andrea Coronetti, *Associate Member, IEEE*, Jean Maël Kempf, Rubén García Alía, *Member, IEEE*, Francesco Cerutti, Daniel Prelipcean, Matteo Cecchetto, Antonio Gilardi, *Member, IEEE*, Wilfrid Farabolini, and Roberto Corsini

***Abstract*— We study the radiation environment near the terahertz (THz) dump of the CERN Linear Electron Accelerator for Research (CLEAR) electron accelerator at CERN, using FLUktuierende KAskade in German (FLUKA) simulations and single-event upset (SEU) measurements taken with 32-Mbit Integrated Silicon Solution Inc. (ISSI) static random access memories (SRAMs). The main focus is on the characterization of the neutron field to evaluate its suitability for radiation tests of electronics in comparison with other irradiation facilities. Neutrons at CLEAR are produced via photonuclear reactions, mostly initiated by photons from the electromagnetic cascades that occur when the beam is absorbed by the dump structure. Good agreement is generally found between the measured single-event upset (SEU) rates and the expected values obtained from FLUKA simulations and the known SEU response of the ISSI SRAMs to neutrons, while one position is found to be potentially affected by photon-driven SEUs.**

***Index Terms*— Accelerator, CERN, CERN Linear Electron Accelerator for Research (CLEAR), electrons, neutrons, photons, photonuclear reactions, radiation effects to electronics (R2E), radiation testing, single-event upsets (SEUs), static random access memories (SRAMs).**

I. Introduction

THE CERN Linear Electron Accelerator for Research (CLEAR) [1] provides electron beams with energies in the 55–220-MeV range, allowing access from both CERN and external users for many applications. In the context of radiation effects to electronics (R2E), direct in-beam irradiations at CLEAR have been used to show that high-energy electrons can induce single-event upsets (SEUs) [2], latchups [3], and stuck bits [4] in memories. This work analyzes the radiation field in off-beam positions near the beam dump of one of the CLEAR test stations, terahertz (THz), with a focus on neutrons generated via photonuclear reactions in the dump block, which are capable of inducing SEUs in sensitive devices via indirect ionization [5]. The goal of the study, which uses Monte Carlo simulations and SEU measurements with static random access memories (SRAMs) [6], is to examine the neutron field properties (flux and energy spectrum) verifying its suitability for radiation testing of devices to be used in present and future CERN accelerators [7], [8] and beyond (e.g., medical applications [9]). In practice, our work consists in verifying that the dump is effectively acting as a target for neutron production, which is a standard approach for the generation of mixed radiation fields in test facilities such as CERN High Energy Accelerator Mixed-field (CHARM) [10], [11] at CERN. While, obviously, the CLEAR radiation field is expected to differ from the one of CHARM, where a 24-GeV proton beam is used, the CLEAR facility presents a number of advantages, linked in particular to the ease of accessing it (CLEAR is a standalone machine, unlike CHARM which is part of the CERN accelerator complex and is hence bound to its operation) and to the flexibility that it offers in terms of beam properties and parameters (e.g., energy, intensity, and time structure).

Manuscript received 8 October 2021; revised 7 February 2022; accepted 1 March 2022. Date of publication 8 March 2022; date of current version 18 July 2022. This work was supported by the European Union's Horizon 2020 Research and Innovation Program through the Marie Skłodowska-Curie Grant under Agreement 721624.

Giuseppe Lerner, Rubén García Alía, Francesco Cerutti, Matteo Cecchetto, and Roberto Corsini are with CERN, CH-1211 Geneva, Switzerland.

Andrea Coronetti is with CERN, CH-1211 Geneva, Switzerland, and also with the Department of Physics, University of Jyväskylä, 40014 Jyväskylä, Finland.

Jean Maël Kempf is with CERN, CH-1211 Geneva, Switzerland, and also with ISAE-Supaero, 31055 Toulouse, France.

Daniel Prelipcean is with CERN, CH-1211 Geneva, Switzerland, and also with the Department of Physics, Technische Universität München, 80333 Munich, Germany.

Antonio Gilardi was with CERN, CH-1211 Geneva, Switzerland, and also with the Department of Physics, University of Naples Federico II, INFN Naples, 80126 Naples, Italy. He is now with the Lawrence Berkeley National Laboratory, Berkeley, CA 94720 USA.

Wilfrid Farabolini is with CERN, CH-1211 Geneva, Switzerland, and also with CEA-Saclay, 91191 Gif-sur-Yvette, France.

Color versions of one or more figures in this article are available at https://doi.org/10.1109/TNS.2022.3157404.

Digital Object Identifier 10.1109/TNS.2022.3157404

II. Experimental Setup

A. CLEAR THz Test Station and Dump

In the present work, we examine the off-beam radiation field near the CLEAR THz test station, which is generated by the direct impact of the high-energy electron beam of CLEAR on the dump, as shown by the pictures in Fig. 1. In particular, to avoid introducing any extra source of radiation, we measure the radiation environment when no device is exposed to the beam in the test area. The dump structure includes a graphite core and a number of iron and concrete blocks, resulting in a total depth of 75 cm, a height of 50 cm above the beam, and a width of 40 cm on its narrower side. While its primary goal is to absorb the electron beam, the impact of the beam on the

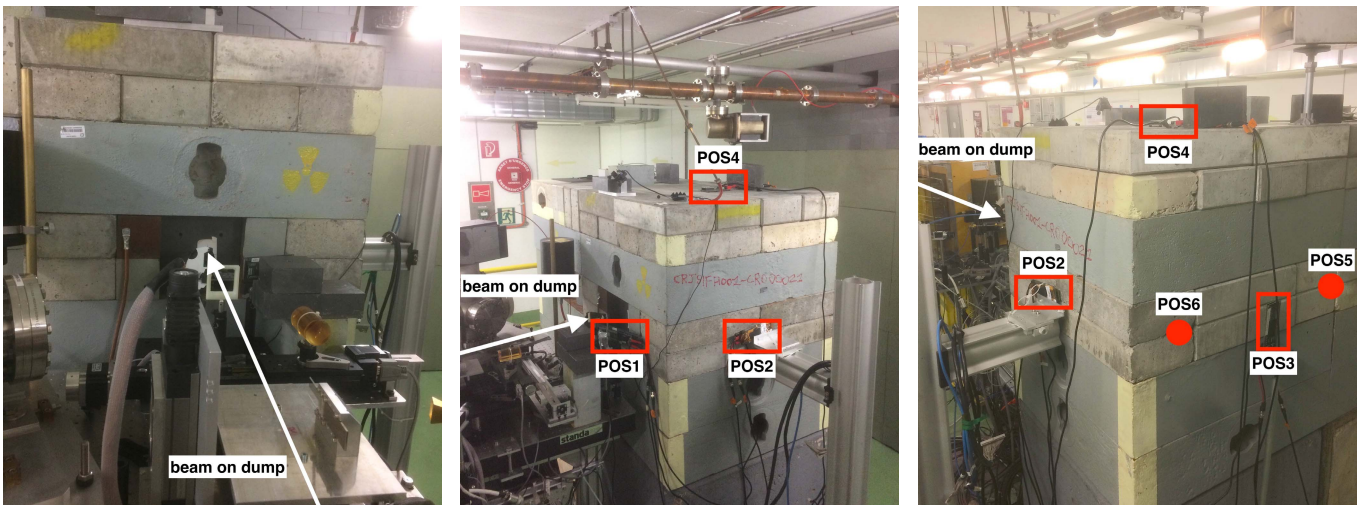

(a) (b) (c)

Fig. 1. (a) Front, (b) side, and (c) back views of the CLEAR THz test station and beam dump, showing the beam axis and the reference test positions where SEU measurements have been taken.

dump generates radiation showers that propagate through its structure and leak in the surrounding environment, resulting in a mixed radiation field that includes mostly electrons, photons, and neutrons produced via photonuclear reactions.

B. ISSI SRAMs as Radiation Monitors

The radiation environment near the CLEAR THz dump has been measured using 32-Mbit Integrated Silicon Solution Inc. (ISSI) SRAM memories as SEU monitors. This represents a standard technique to measure radiation fields in the context of the R2E project, where different types of well-calibrated SRAMs are commonly used for similar purposes (e.g., within the RadMon system [12] deployed in the Large Hadron Collider (LHC) accelerator). Specifically, the choice of ISSI SRAMs is motivated by their relatively high sensitivity to neutrons with energies of the order of the megaelectronvolt (see Section III-D and references therein). During the test, the SRAMs have been placed in six reference positions, all marked in Fig. 1(b) and (c). The first, POS1, is in front of the dump at around 10 cm from the beam axis, behind a small shielding structure that protects a CLEAR beam camera. POS2 and POS4 are, respectively, on the right side and the top of the dump structure, centered with respect to the longitudinal axis. Finally, POS3 is behind the dump on the beam axis, while POS5 and POS6 are 30-cm off-axis in the horizontal direction on the two sides.

C. CLEAR Beam Parameters

While a full description of the CLEAR accelerator performance is available in [13] (including, in particular, all relevant details of the time structure of the beam) Table I presents the key beam parameters of CLEAR for two operational scenarios, both with the electron energy of 205 MeV. The first scenario, corresponding to a realistic high-intensity setting of the accelerator, provides a rate of 6.75×10^{15} electrons on target per hour and is used as a reference to scale the results in this document. The second configuration has a lower charge per train and corresponds to the actual beam intensity that was used to measure the data presented in this document, i.e., 2.70×10^{15} electrons on target per hour, due to the need to be compatible with other ongoing measurements during the same test campaign. In any case, the results presented in this document (i.e., the radiation-level quantities calculated with FLUktuierende KAskade in German (FLUKA) and the measured and expected SEU rates) can be rescaled arbitrarily with the number of electrons on target, and unlike in other cases [14], no effects linked to the intensity rate or the time structure of the beam are present.

TABLE I
BEAM PARAMETERS OF THE CLEAR ACCELERATOR

	High-intensity	Test conditions
Energy [MeV]	205	
Beam FWHM [mm]	5	
Repetition rate [Hz]	10	
Charge per train [nC]	30	12
Electron rate [h^{-1}]	$6.75 \cdot 10^{15}$	$2.70 \cdot 10^{15}$

III. SIMULATION OF THE ENVIRONMENT

The radiation environment is simulated with the Monte Carlo code FLUKA [15]–[17], which provides a detailed description of the particle cascades originating from the interactions of the electron beam with the dump (considering the actual material composition and geometry of the full experimental area) allowing to calculate the quantities of interest for radiation effects to electronics.

A. Photoneutron Production With an Electron Beam

The neutron production at an electron accelerator such as CLEAR occurs predominantly via photonuclear reactions (i.e., nuclear reactions initiated by a bremsstrahlung photon), whereas the direct production of neutrons via electronuclear

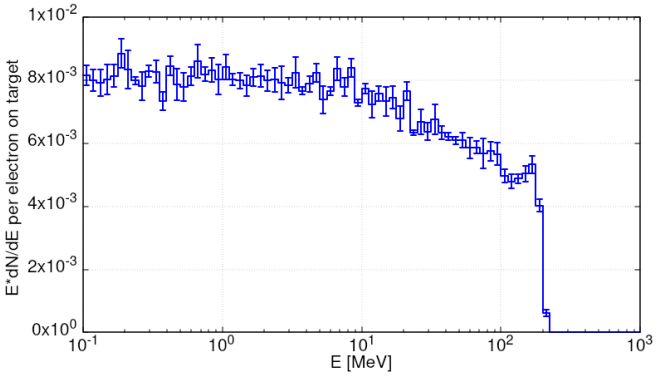

Fig. 2. Simulated distribution per unit lethargy of bremsstrahlung photons produced by a 205-MeV electron beam in a thin (0.1 mm) target made of Fe.

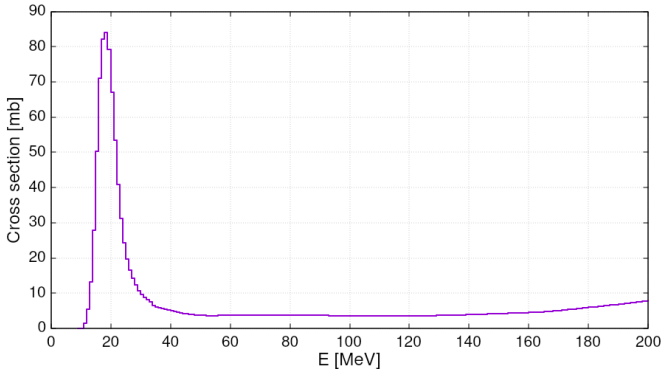

Fig. 3. Total cross section of photonuclear reactions in Fe as a function of photon energy.

reactions (i.e., reactions initiated by an electron and mediated by a virtual photon) is generally subdominant due to their lower cross section [2]. Both processes are modeled in the FLUKA Monte Carlo code [18], which is hence fully capable to simulate the sequence of processes from which most neutrons at CLEAR are originating:

- beam electrons producing photons via bremsstrahlung;
- bremsstrahlung photons producing neutrons via subsequent photonuclear reactions.

The photon production step is shown in Fig. 2, which shows the FLUKA simulation of the energy distribution of photons from a 205-MeV electron beam impacting on a thin (0.1 mm) target made of iron (Fe), which is one of the main components of the CLEAR dump (in addition to graphite and concrete). The distribution, plotted per unit lethargy,[1] is approximately constant up to the beam energy, after which it drops as expected.

Fig. 3 then shows the total cross section for the production of neutrons via photonuclear reactions as a function of the photon energy in Fe. The cross-sectional curve has an important peak around 20 MeV, known as giant dipole resonance (GDR), while at higher photon energies, it stabilizes at a lower and more constant value (mildly increasing above 150 MeV, which is anyway beyond the typical energy range of photons in the CLEAR radiation field, with the exception of few outliers).

Last, Fig. 4 shows the neutron energy distributions resulting from the interaction of monoenergetic photon beams with a thin (0.1 mm) target made of Fe, simulated again with FLUKA. As expected, higher energy photons produce on average higher energy neutrons, but the highest overall yields are reached at neutron energies of the order of few megaelectronvolts and for photon energies corresponding to the GDR cross-sectional peak.

B. FLUKA Model of the Experimental Setup

The geometry of the experimental setup at CLEAR is implemented in FLUKA, and Fig. 5 presents its horizontal 2-D section at beam height, from the extremity of the beam pipe (ending with a 2-mm aluminum window) to the THz beam dump. The latter includes, on the beam axis, a 35-cm-thick and 20-cm-wide graphite core, followed by a 20-cm-thick iron layer and a 20-cm-thick concrete layer. The geometry also includes the smaller shielding element consisting of three bricks of lead and iron in front of the dump, visible in Fig. 1(a) and (b) on the right of the beam axis. Finally, five out of six reference test positions in Fig. 1 are also visible in Fig. 5, while the remaining one, POS4, is above the dump, as shown in Fig. 1.

[1]In lethargy spectra, the energy bins on the x-axis are in logarithmic scale and the y-axis shows the differential yield per unit logarithm of the energy, such that when the y-axis is in linear scale, equal areas below the curve correspond to equal particle yields.

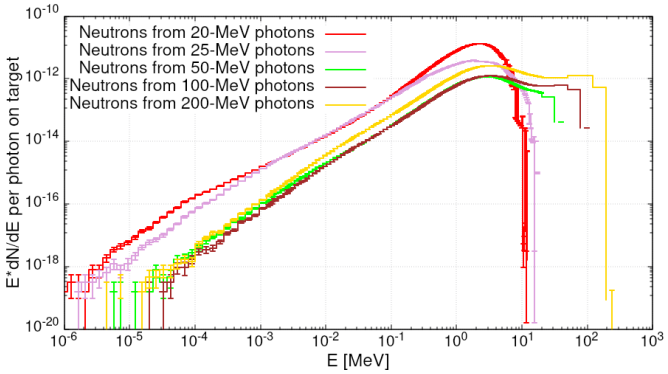

Fig. 4. Photoneutron distribution per unit lethargy simulated with FLUKA for photons of different energies impacting on a target made of Fe.

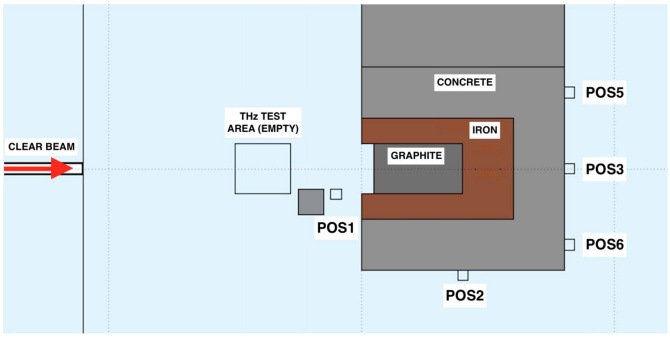

Fig. 5. Horizontal 2-D section of the FLUKA geometry at beam height with five test positions indicated by small boxes.

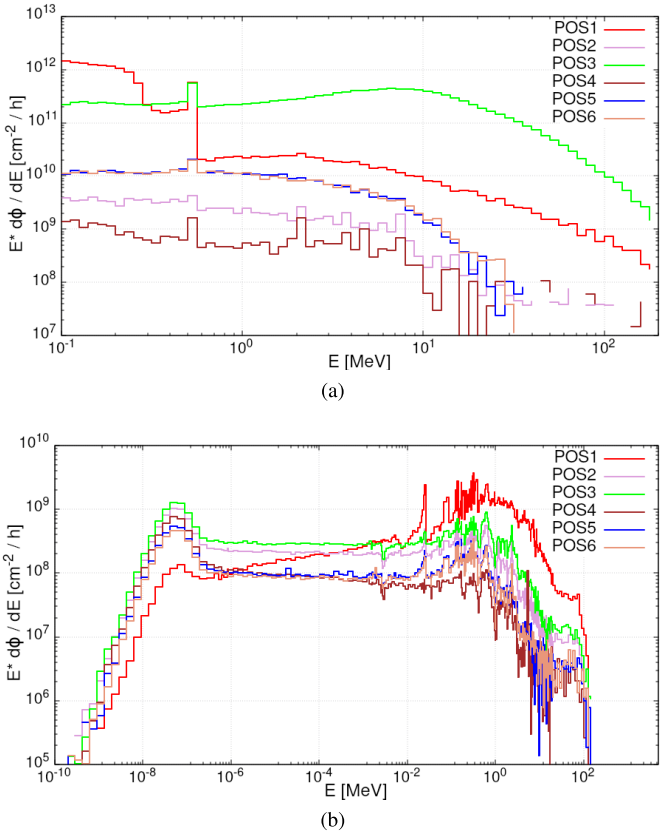

Fig. 6. Simulated distributions of (a) photons and (b) neutrons per unit lethargy in the reference test positions at CLEAR.

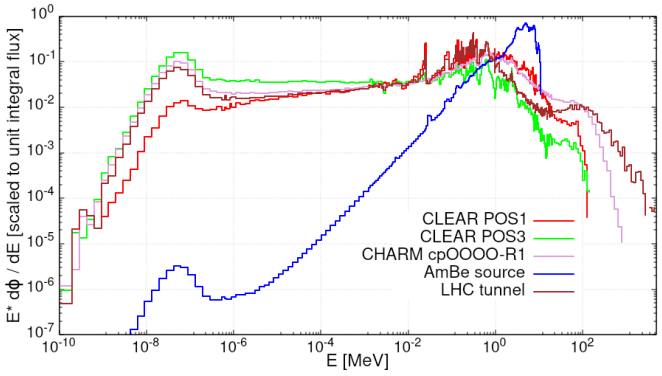

Fig. 7. Comparison between two neutron spectra at CLEAR and analogous neutron spectra at the CHARM (for a copper target, in the lateral R1 position without shielding) and AmBe facilities and in the LHC tunnel at CERN.

C. Particle Energy Spectra at CLEAR

The energy distributions of neutrons and photons in the six reference test positions are shown in Fig. 6, plotted per unit lethargy. Compared to the spectrum shown in Fig. 4, in all test positions at CLEAR, there is a thermal neutron peak due to the presence of low-Z materials (particularly hydrogen in concrete) that thermalize the neutrons. In addition, the neutron spectra peak around 1 MeV and drop significantly above 10 MeV, with the partial exception of POS1 (i.e., the dump front) where the energy distribution is more shifted toward higher energies compared to the other positions. The fact that the neutron energy spectrum peaks around 1 MeV has important consequences for SEU measurements due to the variable SEU cross sections of different electronic devices in this neutron energy range [19], as further described in the next paragraph. It should also be noted that the photon flux is particularly high in POS3, while it is lower in other positions (again with the partial exception of POS1), especially above 10 MeV.

Finally, Fig. 7 presents a comparison between the neutron energy spectrum in POS1 and POS3 at CLEAR and three reference neutron spectra obtained again from FLUKA simulations, namely, an AmBe source, a reference position at CHARM with a standard copper target and no lateral shielding, and a portion of the LHC tunnel in proximity of one of its main experiments [20]. The differences in the thermal neutron flux peak can be neglected, as the thermal peak can easily be enhanced or suppressed by using dedicated moderators or shieldings (in fact, the AmBe source at CERN is placed on purpose in an area that minimizes the thermalization process of neutrons). Instead, it is interesting to focus on the comparison of the energy distributions at the MeV scale and above. In particular, the CLEAR neutrons reach higher energies compared to the AmBe ones (although the flux peaks at lower energy), while, as expected, the maximum energies at CHARM and (even more) at the LHC are higher. The AmBe spectrum, together with neutron spectra in a number of other facilities and radiation fields, is further described in [19].

D. Radiation-Level Calculations

Since the key goal of this document is the measurement of the SEU rate at CLEAR with SRAMs, the radiation field is mapped using a set of quantities that allow to predict it under the high-energy hadron (HEH) approximation [21].

1) *HEH-eq Flux:* Hadrons with $E > 20$ MeV plus neutrons of intermediate energy (typically from a fraction of megaelectronvolts up to the 20-MeV threshold) weighted with a Weibull response function with device-specific parameters, as further described below;
2) *Thermal Neutron Equivalent Flux:* The equivalent flux of 25-meV neutrons with weights proportional to the inverse of the neutron velocity;
3) *$E > 10$ MeV Photon and $E > 10$ MeV Electron Fluxes:* Proportional in first approximation to the expected rate of photon- and electron-induced SEUs, respectively, where the former quantity is more relevant due to the higher cross section of photonuclear reaction as opposed to electronuclear ones [2].

Notably, since the neutron spectrum at CLEAR [see Fig. 6(b)] peaks in the intermediate-energy region, the HEH-eq flux depends significantly on the device-specific Weibull coefficients that parameterize the dependence of the neutron-induced SEU cross section with energy in this range

$$\sigma(E) = \sigma_{\text{sat}}\left[1 - e^{-((E-E_0)/W)^s}\right]. \quad (1)$$

The parameters in the exponential in (1), together with the saturation cross sections σ_{sat}, are reported in Table II for

TABLE II

HEH SEU CROSS SECTION AND WEIBULL PARAMETERS OF 32-Mbit ISSI (DATE CODE 1650) AND 4-Mbit TOSHIBA SRAMS [19]

	σ_{sat}^{HEH} [cm^2/bit]	E_{th} [MeV]	W [MeV]	s
Toshiba	$6.6 \cdot 10^{-14}$	0.2	9.25	3.02
ISSI	$1.4 \cdot 10^{-14}$	0.01	14.05	0.82

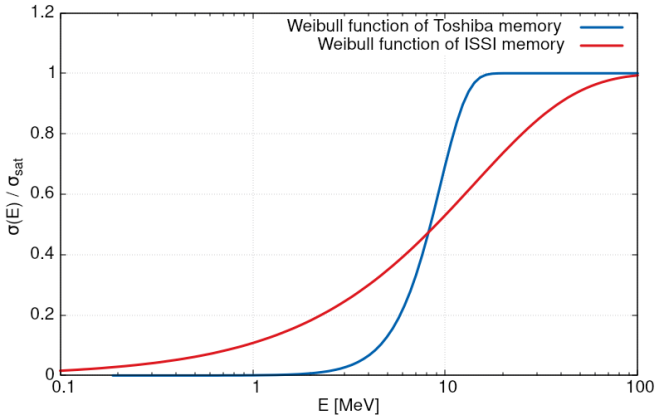

Fig. 8. Weibull functions of the Toshiba and ISSI memories, obtained through (1) with the parameters in Table II.

a standard Toshiba SRAM and for the ISSI used in our test. The resulting $\sigma(E)/\sigma_{sat}$ curves are shown in Fig. 8; as anticipated, the ISSI was chosen due to its higher sensitivity to megaelectronvolt-scale neutrons,[2] due to its more integrated technology and smaller critical charge [18], whereas Toshiba can be considered as a reference and is employed for further discussions in Section IV. The thermal neutron SEU cross section of the ISSI SRAMs is also available in the literature ($\sigma_{th} = 3.2 \times 10^{-15}$ cm^2 [22]), whereas the photon-induced SEU cross section of the ISSI is unknown, although from the simulation studies in [2], we expect that it is substantially lower than the neutron one (with the electron SEU cross section being even lower).

In addition, and for the purpose of completeness, in this paragraph, we also present the FLUKA predictions of two quantities linked to cumulative damage to electronic equipment and materials as follows:

1) total ionizing dose (TID), i.e., the energy deposited by the radiation field via ionization, measured in gray (Gy) with 1 Gy = 1 J/kg;
2) silicon 1-MeV neutron equivalent flux (1-MeV n-eq), proportional to the displacement damage (DD) produced by the radiation field in a silicon lattice, with contribution of each particle weighted according to its relative impact compared to 1-MeV neutrons.

The simulated HEH-eq flux with the Weibull parameters of the ISSI SRAMs, the thermal neutron equivalent flux, and

[2]While the Weibull function of the ISSI is substantially higher than the one of the Toshiba at the megaelectronvolt scale, the ISSI curve increases less steeply beyond a few MeV, with full saturation occurring beyond the standard 20-MeV threshold. However, since the neutron energy spectra at CLEAR peak at the megaelectronvolt scale, this feature has a minor impact on the results in the present document.

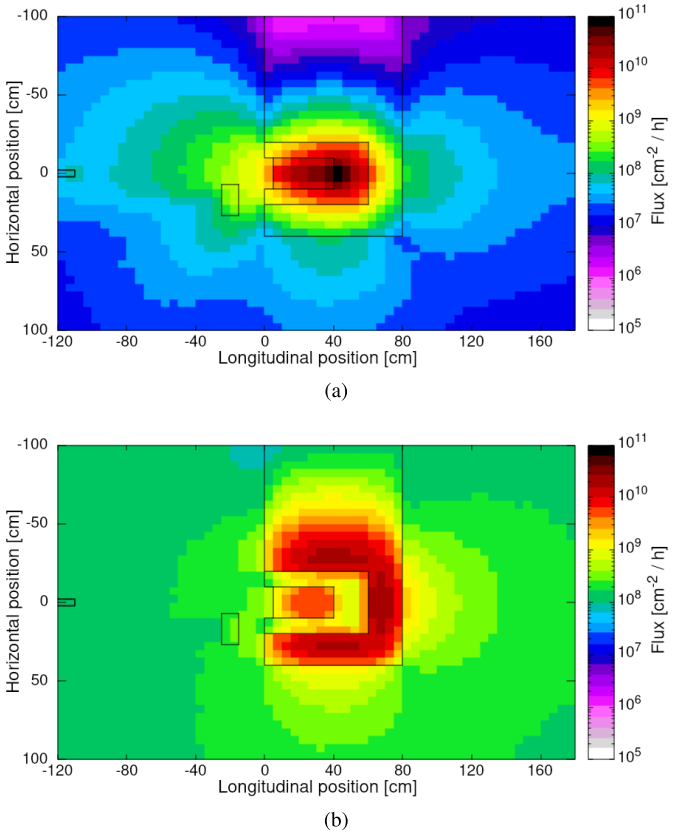

Fig. 9. (a) Top view of ISSI HEH-eq flux and (b) thermal neutron equivalent flux at beam height.

the $E > 10$ MeV photon and electron fluxes are shown in Figs. 9 and 10 as top views at beam height for 1 h of high-intensity beam operation. The HEH-eq and thermal fluxes are quite uniformly distributed around the dump, while the $E > 10$ MeV photon and electron fluxes have a more conical shape centered on the beam axis, implying that they are relatively more abundant behind the dump (particularly on the beam axis) compared to the dump side (and top). The iron layer suppresses the thermal neutrons inside the dump, but their flux recovers significantly in the surrounding concrete blocks.

The corresponding plots of the quantities associated with cumulative damage, i.e., TID and 1-MeV n-eq, are instead shown in Fig. 11, where the shape of the TID distribution presents a similar conical shape to the $E > 10$ MeV photon and electron fluxes, reflecting the fact that the majority of the energy is deposited by electromagnetic showers. The large values of both TID and 1-MeV n-eq flux along the beam axis are expected due to the primary beam electrons that are also contributing to the 1-MeV n-eq flux (albeit with a relatively small weight) because they are known to cause a nonnegligible amount of DD.

IV. TEST RESULTS

A. SEU Measurements

The SEU rate has been measured with 32-Mbit ISSI SRAMs in the six positions in Fig. 1. The measurements have been

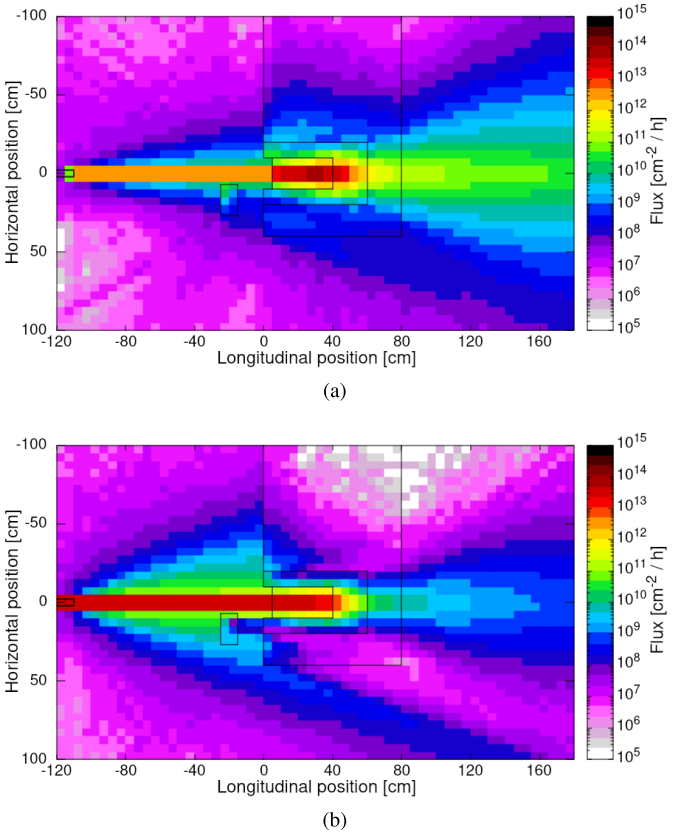

Fig. 10. Top view of $E > 10$ MeV: (a) photon and (b) electron fluxes at beam height.

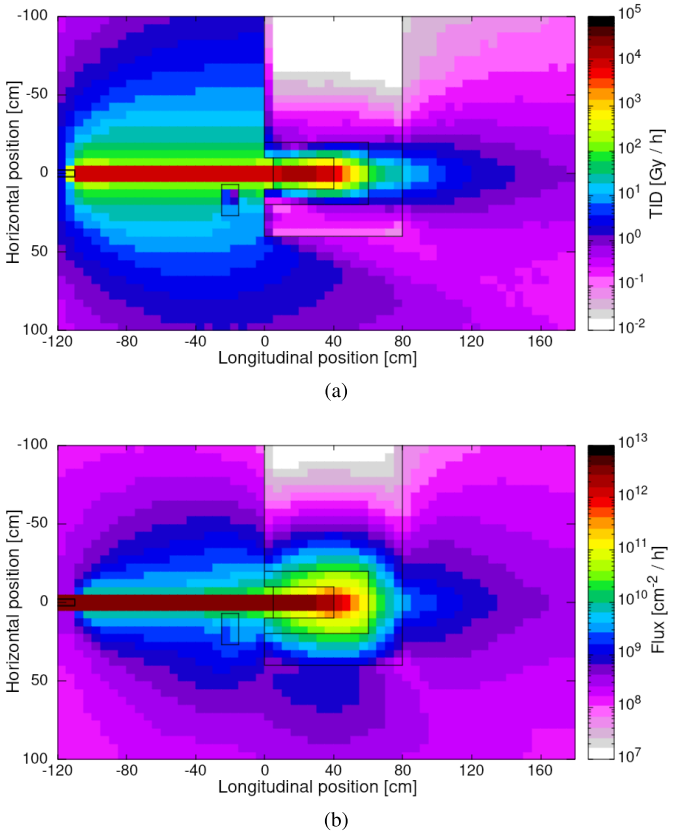

Fig. 11. (a) Top view of TID and (b) silicon 1-MeV neutron equivalent flux at beam height.

performed with and without a boron carbide (B_4C) lid that shields the SRAMs from thermal neutrons, to be able to quantify the respective contribution of HEH-eq flux and thermal neutron equivalent flux to the total counts. The results are summarized in Table III (top part) rescaled to 1 h of high-intensity CLEAR performance from Table I in order to show the maximum rates that can be reached in analogous test conditions. The uncertainty on the observed SEU rates reflects the statistical (Poisson) error on the raw counts during the test, which took place at the lower beam intensity presented in Table I.

B. Comparisons With FLUKA-Based Predictions

In addition to the data, the first part of Table III also includes the FLUKA predictions of HEH-eq and thermal neutron equivalent fluxes, together with the expected SEU yields based on the ISSI cross section from HEHs and thermal neutrons (see Section III-D and, in particular, Table II). The thermal neutron component is not considered when predicting the SEU yield for the configurations with B_4C lid (i.e., assuming a 100% shielding efficiency), while any contribution from other particles (particularly photons) is not considered due to the unknown SEU cross section (which is anyway expected to be much lower than the HEH-eq and thermal ones, as discussed in the previous paragraphs). In addition, the second part of the table presents the FLUKA predictions of the remaining quantities of interest for radiation effects, namely, the TID,

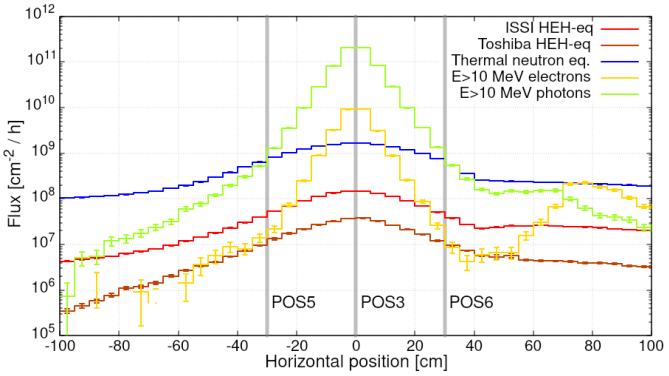

Fig. 12. Flux profiles versus horizontal position behind the CLEAR dump.

the silicon 1-MeV neutron equivalent flux, and the $E > 10$ MeV photon and electron fluxes. In terms of uncertainties, the FLUKA predictions of the various quantities are expected to be accurate from the point of view of the physics models, while some inconsistencies in the predictions may be present due to the simplified geometry model of the facility, although the main elements have been carefully implemented. The cross sections used to calculate the expected SEU yields represent an extra source of uncertainty such that, overall, we can expect to reproduce the measured rates within approximately ±50%.

Indeed, the expected and measured SEU yields are generally consistent within a factor 2 or less, with only one notable exception in the case of POS3, as further discussed in the

TABLE III

SUMMARY OF THE RESULTS OF THE CLEAR TEST CAMPAIGN IN COMPARISON WITH THE FLUKA PREDICTIONS, SCALED TO THE HIGH-INTENSITY CLEAR SETTINGS IN TABLE I. THE FIRST TABLE SHOWS THE MEASURED DATA AND THE EXPECTED SEU YIELDS, AS PREDICTED FROM FLUKA SIMULATIONS OF HEH-EQ AND THERMAL NEUTRON EQUIVALENT FLUX AND FROM THE SEU CROSS SECTIONS DESCRIBED IN SECTION III-D. THE FLUKA PREDICTIONS OF THE REMAINING QUANTITIES OF INTEREST ARE PRESENTED IN THE SECOND TABLE

Position	B_4C lid	ISSI HEH-eq flux	thermal n-eq flux	N_{SEU}^{pred}/h	N_{SEU}^{obs}/h	observed/predicted SEU ratio
POS1	No	$7 \cdot 10^8$ cm^{-2}/h	$3 \cdot 10^8$ cm^{-2}/h	361	364 ± 23	1.0
	Yes		not considered	329	433 ± 21	1.3
POS2	No	$9 \cdot 10^7$ cm^{-2}/h	$1.5 \cdot 10^9$ cm^{-2}/h	203	282 ± 20	1.4
	Yes		not considered	42	79 ± 9	1.9
POS3	No	$1.5 \cdot 10^8$ cm^{-2}/h	$1.5 \cdot 10^9$ cm^{-2}/h	232	483 ± 26	2.1
	Yes		not considered	70	446 ± 22	6.3
POS4	No	$2 \cdot 10^7$ cm^{-2}/h	$1 \cdot 10^9$ cm^{-2}/h	117	102 ± 12	0.9
	Yes		not considered	9.4	15 ± 4	1.6
POS5	No	$4.5 \cdot 10^7$ cm^{-2}/h	$7 \cdot 10^8$ cm^{-2}/h	96	99 ± 8	1.0
	Yes		not considered	21	34 ± 5	1.6
POS6	No	$4.5 \cdot 10^7$ cm^{-2}/h	$6 \cdot 10^8$ cm^{-2}/h	n.a.	n.a.	n.a.
	Yes		not considered	21	28 ± 4	1.3

Position	TID	1-MeV n-eq flux	E>10 MeV photon flux	E>10 MeV electron flux
POS1	1 Gy/h	$1 \cdot 10^{10}$ cm^{-2}/h	$5 \cdot 10^9$ cm^{-2}/h (high gradient)	$1 \cdot 10^{10}$ cm^{-2}/h (very high gradient)
POS2	0.4 Gy/h	$7.5 \cdot 10^8$ cm^{-2}/h	$2.5 \cdot 10^8$ cm^{-2}/h	$3 \cdot 10^7$ cm^{-2}/h
POS3	14 Gy/h	$3 \cdot 10^9$ cm^{-2}/h	$2 \cdot 10^{11}$ cm^{-2}/h	$1 \cdot 10^{10}$ cm^{-2}/h
POS4	0.3 Gy/h	$1.5 \cdot 10^8$ cm^{-2}/h	$1 \cdot 10^8$ cm^{-2}/h	$2 \cdot 10^8$ cm^{-2}/h
POS5	0.3 Gy/h	$4 \cdot 10^8$ cm^{-2}/h	$8 \cdot 10^8$ cm^{-2}/h	$2 \cdot 10^7$ cm^{-2}/h
POS6	0.3 Gy/h	$4 \cdot 10^8$ cm^{-2}/h	$8 \cdot 10^8$ cm^{-2}/h	$3 \cdot 10^7$ cm^{-2}/h

following. Consistently with the predictions, and apart from POS1 where the thermal neutron component is small, the SEU yield decreases when the B_4C lid is applied. The systematic increase of the observed versus predicted ratio with the B_4C lid may indicate a mild overestimation of the thermal neutron equivalent flux in the FLUKA simulation, which is not unrealistic due to the high sensitivity of this quantity to factors such as the exact concrete composition (in particular, the hydrogen content) that are not trivial to reproduce accurately in the geometry model of the simulation.

As anticipated, a large deviation from the FLUKA predictions is observed in POS3, particularly with the B_4C lid (i.e., when any contribution from thermal neutrons is removed). A potential explanation for this large disagreement can be found by examining Fig. 12, which shows the horizontal 1-D profile of the relevant particle fluxes as a function of the horizontal position, including POS3, POS5, and POS6. From the figure, it is clear that the ratio of $E > 10$ MeV photon flux versus thermal neutron and HEH flux peaks on the beam axis (i.e., in POS3) and decreases rapidly on both sides (i.e., in POS5 and POS6) reflecting the different shape of electromagnetic and hadronic radiation fields already seen in Figs. 9–11 and coherently with the FLUKA predictions in Fig. 6(a) and Table III. As a consequence, even if the photon SEU cross section is expected to be substantially lower than the HEH-eq and thermal ones, the $E > 10$ MeV photon flux peak may result in nonnegligible (or even dominant) photon-induced SEU counts, especially in POS3. While this prediction cannot be further verified without knowing the photon SEU cross section of the ISSI SRAM, it is possible to affirm that the measurements in Table III are qualitatively coherent with it.

Last, Fig. 12 includes two 1-D HEH-eq flux profiles: one based on the Weibull parameters of the ISSI memories used in the test (and presented also elsewhere throughout this document) and one based on the corresponding parameters of a Toshiba memory that has lower sensitivity to megaelectronvolt-scale neutrons. The Toshiba HEH-eq flux is found to be lower by at least a factor 3 compared to the ISSI one, confirming that intermediate-energy neutrons (i.e., neutrons with energy ranging from fractions of 1 up to 20 MeV) represent effectively its dominant component and that that the CLEAR facility is particularly suitable to test devices that are highly sensitive to them.

V. CONCLUSION

The main highlight of this work is the experimental confirmation of the presence of a significant neutron field near the CLEAR THz dump, suitable for SEU measurements with SRAMs. The neutron energy spectrum extends from thermal to high energies (up to $\sim$100 MeV) with a peak around 1 MeV such that the HEH-eq flux is dominated by intermediate-energy neutrons, implying that the SEU rates are affected by the associated device-specific response. Additional test campaigns involving different devices or, possibly, different types of SEE (e.g., single-event latchups or burnouts) can be planned in the future to assess the suitability of the CLEAR facility for a broader range of R2E-related activities.

During our test, the highest rate of SEUs has been observed in POS1 and POS3, with different caveats; the SEU rate in POS1 is particularly sensitive to beam settings (e.g., the width) and to showers generated locally by the presence of elements in the test area, while in POS3, we found the highest discrepancy between observed and predicted SEU rate, possibly due to photon-induced SEUs, as described in Section IV-B. The remaining test positions yield a more stable SEU rate, in good agreement with the predictions based on the FLUKA simulations and the SEU cross section of the ISSI SRAMs. Compared to other facilities (e.g., CHARM), the HEH-eq flux rates at CLEAR are lower, and however, they can still be considered sufficient to test components or systems for relatively low radiation areas and even more so if the devices are highly sensitive to intermediate-energy neutrons. For practical applications, we can recommend to employ POS2, POS4, POS5, or POS6 in order to have a well-benchmarked radiation environment, whereas POS3 can be exploited to obtain a higher rate of SEEs, knowing that they may originate not only from neutrons but possibly also from other particles (most likely photons).

Given that the present work has successfully demonstrated the possibility to measure SEUs using the CLEAR beam dump as target, as a future development, it is interesting to consider the development of a dedicated target for photoneutron production, to be placed directly on the primary CLEAR beam. This may allow to further optimize the neutron field properties (e.g., the energy spectrum) and to enhance the rate of the radiation level quantities of interest reported in this document.

REFERENCES

[1] M. Brugger *et al.* (2016). *The CLEAR Facility at CERN*. [Online]. Available: https://cds.cern.ch/record/2311397

[2] M. Tali *et al.*, "High-energy electron-induced SEUs and Jovian environment impact," *IEEE Trans. Nucl. Sci.*, vol. 64, no. 8, pp. 2016–2022, Aug. 2017.

[3] M. Tali *et al.*, "Mechanisms of electron-induced single-event latchup," *IEEE Trans. Nucl. Sci.*, vol. 66, no. 1, pp. 437–443, Jan. 2019.

[4] D. Soderstrom *et al.*, "Electron-induced upsets and stuck bits in SDRAMs in the Jovian environment," *IEEE Trans. Nucl. Sci.*, vol. 68, no. 5, pp. 716–723, May 2021.

[5] K. Roed *et al.*, "FLUKA simulations for SEE studies of critical LHC underground areas," *IEEE Trans. Nucl. Sci.*, vol. 58, no. 3, pp. 932–938, Jun. 2011.

[6] A. Coronetti *et al.*, "SEU characterization of commercial and custom-designed SRAMs based on 90 nm technology and below," in *Proc. IEEE Radiat. Effects Data Workshop (NSREC)*, Nov. 2020, pp. 56–63.

[7] O. Aberle *et al.*, "High-luminosity large Hadron collider (HL-LHC): Technical design report," CERN Yellow Reports: Monographs, Geneva, Switzerland, Tech. Rep. CERN-2020-010, 2020.

[8] M. Benedikt *et al.*, "FCC-EE: The Lepton collider: Future circular collider conceptual design report volume 2. Future circular Collider," Geneva, Switzerland, Tech. Rep. CERN-ACC-2018-0057, Dec. 2018.

[9] D. S. Followill, F. Nüsslin, and C. G. Orton, "IMRT should not be administered at photon energies greater than 10MV," *Med. Phys.*, vol. 34, no. 6, pp. 1877–1879, May 2007.

[10] J. Mekki, M. Brugger, R. G. Alia, A. Thornton, N. C. Dos Santos Mota, and S. Danzeca, "CHARM: A mixed field facility at CERN for radiation tests in ground, atmospheric, space and accelerator representative environments," *IEEE Trans. Nucl. Sci.*, vol. 63, no. 4, pp. 2106–2114, Aug. 2016.

[11] A. Infantino *et al.*, "Dose gradient assessment at the new CERN CHARM irradiation facility," *Radiat. Phys. Chem.*, vol. 155, pp. 225–232, Feb. 2019.

[12] G. Spiezia *et al.*, "A new RadMon version for the LHC and its injection lines," *IEEE Trans. Nucl. Sci.*, vol. 61, no. 6, pp. 3424–3431, Dec. 2014.

[13] K. Sjobak *et al. Status of the CLEAR Electron Beam User Facility at CERN*. CERN-ACC-2019-084. Accessed: Mar. 1, 2021. [Online]. Available: https://cds.cern.ch/record/2695092

[14] V. Wyrwoll *et al.*, "Highly pulsed electron beam induced SEU effects in a SRAM memory," in presented at RADECS 2021, Vienna, Austria, Sep. 2021.

[15] *FLUKA Website*. Accessed: Mar. 1, 2021. [Online]. Available: https://fluka.cern

[16] G. Battistoni *et al.*, "Overview of the FLUKA code," *Ann. Nucl. Energy*, vol. 82, pp. 10–18, Aug. 2015.

[17] T. T. Böhlen *et al.*, "The FLUKA code: Developments and challenges for high energy and medical applications," *Nucl. Data Sheets*, vol. 120, pp. 211–214, Apr. 2014.

[18] A. Fassò, "Photonuclear reactions in FLUKA: Cross sections and interaction models," in *Proc. AIP Conf.*, 2005, p. 1303.

[19] M. Cecchetto *et al.*, "0.1–10 MeV neutron soft error rate in accelerator and atmospheric environments," *IEEE Trans. Nucl. Sci.*, vol. 68, no. 5, pp. 873–883, May 2021.

[20] D. Prelipcean, "Comparison between measured radiation levels and FLUKA simulations at CHARM and in the LHC tunnel of P1-5 within the R2E project in Run 2," M.S. thesis, Dept. Phys., Technische Universität München, CERN-THESIS-2021-101, 2021.

[21] K. Roeed *et al.*, "Method for measuring mixed field radiation levels relevant for SEEs at the LHC," *IEEE Trans. Nucl. Sci.*, vol. 59, no. 4, pp. 1040–1047, Aug. 2012.

[22] M. Cecchetto *et al.*, "Thermal neutron-induced SEUs in the LHC accelerator environment," *IEEE Trans. Nucl. Sci.*, vol. 67, no. 7, pp. 1412–1420, Jul. 2020.